ISSN 1990-7931, Russian Journal of Physical Chemistry B, 2015, Vol. 9, No. 6, pp. 983–991. © Pleiades Publishing, Ltd., 2015.
Original Russian Text © D.S. Kotova, V.E. Zakharov, M.V. Klimenko, V.V. Klimenko, 2015, published in Khimicheskaya Fizika, 2015, Vol. 34, No. 12, pp. 62–71.

CHEMICAL PHYSICS OF ATMOSPHERIC PHENOMENA

Development of the Model of HF Radiowave Propagation in the Ionosphere[1]

D. S. Kotova[a, b, *], V. E. Zakharov[a], M. V. Klimenko[a, b], and V. V. Klimenko[b]

[a] *Baltic Kant Federal University, Kaliningrad, Russia*

[b] *Institute of Terrestrial Magnetism, Ionosphere, and Radiowave Propagation, Western Division, Russian Academy of Sciences, pr. Pobedy 41, Kaliningrad, 236017 Russia*

**e-mail: darshu@ya.ru*

Received December 11, 2014

Abstract—The model of HF radiowave propagation, based on a geometrical optics approximation, has been extended for the case of a complex geometrical optics. The radiowave propagation in the illuminated region without going to the caustic shadow region is considered. The radiowave propagation model has been generalized for the case of wideband HF signals in the ionosphere. A dynamic representation of LFM signals in the form of a wave packet sequence was used for this purpose. The radiowave propagation model was also adapted to a global self-consistent dynamic model of the thermosphere, ionosphere, and protonosphere, which made it possible to study specific features in the formation of HF radiowave ray paths during geomagnetic storms in a 3D inhomogeneous anisotropic medium.

Keywords: complex geometric optics, LFM pulse, radiowave attenuation, HF propagation, geomagnetic storms, numerical simulation

DOI: 10.1134/S1990793115050218

INTRODUCTION

In the last decade, HF radio paths have been studied simultaneously using different numerical models of the ionosphere and radiowave propagation [1–5]. Apparent advantages of the results achieved in these works are as follows: (1) a model description of the radiowave propagation in the main ionospheric trough region [1, 2]; (2) the construction of model oblique ionograms with the following interpretation of experimental ionograms [3, 4]; (3) model studying the main characteristics of oblique ionograms [5]. However, these studies have their own limitations. They use either a high-latitude ionosphere model or a model of the ionosphere–plasmasphere system ignoring the low-latitude region, which are not global 3D models and do not make it possible to calculate the electric field and thermospheric and ionospheric parameters in a self-consistent manner.

The specific feature of our studies consists in performing numerical calculations of HF radiowave trajectories in a 3D inhomogeneous anisotropic ionosphere, which is modeled based on a global self-consistent model of the thermosphere, ionosphere, and protonosphere (GSM TIP) [6, 7]. The used radiowave propagation (RWP) model was developed in [8]. This model is complex and universal. The aim of this work is to indicate the possibilities of the RWP model developed by us.

1. RP MODEL

In the initial state, the RWP numerical model [8] was constructed by solving the eikonal equation using the method of characteristics for either normal wave mode based on a geometrical optics approximation [9]. The solution was reduced to integrating the system of ray equations for coordinates and pulses:

$$\begin{cases} d\mathbf{r}/d\tau = \mathbf{p} - n\partial n/\partial \mathbf{p} \equiv \mathbf{s}(\mathbf{r}, \mathbf{p}), \\ d\mathbf{p}/d\tau = n\partial n/\partial \mathbf{r}, \end{cases}$$

where τ is the parameter of integration along each ray path; $\mathbf{p}$ and $\mathbf{s}$ are the pulse and ray vectors, respectively; $\mathbf{r}$ is the radius vector of the observation point on a ray; n is the refractive index of a medium.

The complex parameters of refraction of ordinary and extraordinary waves at ionospheric altitudes from 60 to 1000 km were calculated using the cold plasma permittivity tensor [10]. The differential absorption ratio for either normal mode was expressed by the formula

$$k_{\text{dif}}\,[\text{dB m}^{-1}] = 8.68(\omega/c)\,\text{Im}(n),$$

where ω is the oscillation frequency, and c is the velocity of light.

[1] This article was presented as a paper at the IV International conference "Atmosphere, Ionosphere, Safety" (Zelenogradsk, Kaliningradskaya oblast, Russia, 2014).

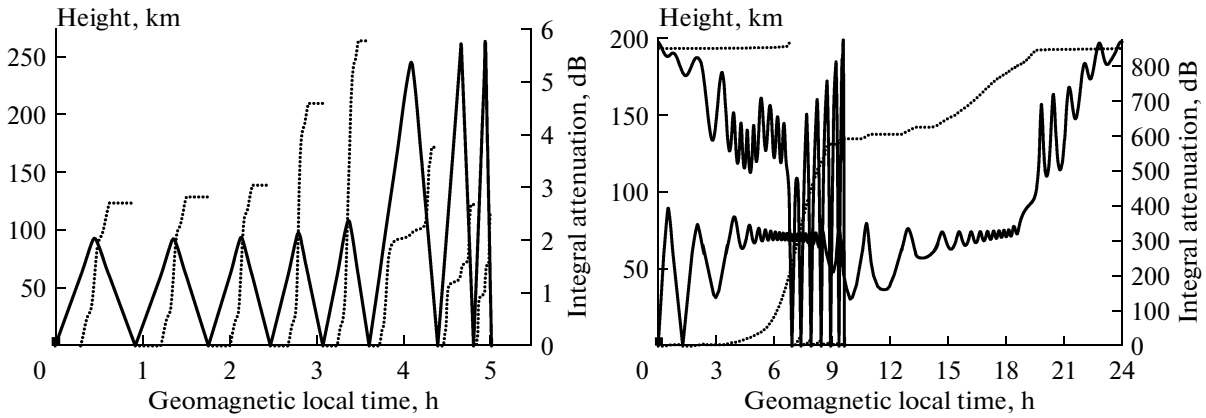

Fig. 1. Numerical calculation results for the paths and integral absorption of HF radiowaves in the ionosphere ($f = 5$ MHz, $\alpha = 15°$, $\beta = 90°$, $\varphi = 55°$ N, $\lambda = 70°$ W, 04:39 UT) for ordinary (left) and extraordinary (right) wave modes.

The integral absorption (in dB) along each ray on a distinguished segment of each ray path (from σ_0 to σ) was found using the formula

$$k_{\text{int}} = \int_{\sigma_0}^{\sigma} k_{\text{dif}} \cos\gamma d\sigma,$$

where γ is the angle between vectors **s** and **p**.

Figure 1 illustrates the application of the RWP numerical model for the calculation of multihop ray paths and radiowave attenuation in the ionosphere [11]. The ray paths of ordinary (left) and extraordinary (right) waves are shown in geomagnetic local time–height above the Earth's surface coordinates. The plots of absorption of ordinary and extraordinary waves (dotted lines) are shown in geomagnetic local time–integral absorption along each one-hop path over the Earth's surface coordinates. We considered the radiowave propagation under the summer solstice conditions. We specified the parameters necessary for calculating the medium refractive index using the IRI (International Reference Ionosphere [12]) empirical model of the ionosphere. The transmitting station location on the Earth's surface is marked by a square in Fig. 1. We accepted the following denotations: α and β are the transmitter elevation angle and emission azimuth, respectively; φ and λ are the transmitter geographic latitude and longitude, respectively; f is frequency. The calculations indicated that the average curvature radius increases in going from the dayside to nightside of the ionosphere along each ray path altitude; as compared to ordinary waves, it may be more difficult to register extraordinary wave signals during their multihop propagation since they are more intensely absorbed in ionosphere; the HF radiowave energy absorption is most intense under daytime conditions at altitudes of the ionospheric D and E regions.

2. MODEL DEVELOPMENT FOR THE CASE OF COMPLEX GEOMETRICAL OPTICS

The complex geometrical optics method can be used to describe inhomogeneous waves in anisotropic mediums with weak absorption and potentially attenuating waves in the caustic shadow region [13]. The radiowave propagation model has been developed for the case of a complex geometrical optics with real ray paths [14]. The condition

$$\text{Im}\,\mathbf{r} = 0 \tag{1}$$

is valid for the corresponding ray paths. This expression makes it possible to find ray paths in an illuminated region without entering into the geometrical shadow region.

The dispersion relation in a local approximation for either normal mode has the form [13]

$$H(\mathbf{p},\mathbf{r}) = \frac{1}{2}\left[\mathbf{p}^2 - n^2(\mathbf{r},\mathbf{l})\right] = 0, \tag{2}$$

where H is the system Hamiltonian, **p** is the complex pulse, n is the complex refractive index of a medium, and **l** is the complex vector of the normal to the wave phase front. In this case $\mathbf{p} = p\mathbf{l}$, where p is the pulse complex value, and $\mathbf{l}^2 = 1$ so that $p = n$.

In generalized coordinates instead of system (2) and (1) we have

$$H(p_i, q_i) = 0, \tag{3}$$

$$\text{Im}\, q_i = 0, \tag{4}$$

where $i = 1, 2, 3$; and p_i is the pulse conjugate to coordinate q_i.

We use the method of characteristics in order to solve system (3), (4). The relationship

$$dH = \sum_{i=1}^{3}\left(\frac{\partial H}{\partial p_i}dp_i + \frac{\partial H}{\partial q_i}dq_i\right) = 0 \tag{5}$$

is satisfied on hypersurface (3) in phase space (p_i, q_i).

Relationship (5) is valid identically if

$$\frac{dq_i}{\partial H/\partial p_i} = -\frac{dp_i}{\partial H/\partial q_i} = d\tau_i, \tag{6}$$

where $d\tau_i$ is the differential of a certain complex function τ_i, which changes during a motion along each distinguished characteristic.

Expression (6) results in the set of equations for determining the characteristics:

$$dq_i/d\tau_i = \partial H/\partial p_i, \quad dp_i/d\tau_i = -\partial H/\partial q_i. \tag{7}$$

Having expressed dq_i from (7) and having substituted it into (4), we obtain

$$\mathrm{Im}\ dq_i = \mathrm{Im}\left(\frac{\partial H}{\partial p_i} d\tau_i\right) = 0. \tag{8}$$

The algebraic representation of differential $d\tau_i$ gives

$$d\tau_i = d\tau + j d\tau_i', \tag{9}$$

where τ is the independent variable.

Having substituted (9) into (8), we have

$$d\tau_i' = -\frac{\mathrm{Im}(\partial H/\partial p_i)}{\mathrm{Re}(\partial H/\partial p_i)} d\tau. \tag{10}$$

We substitute (10) into (9) and the result into (7). Taking (8) into account, we find the system of equations for determining the characteristics:

$$\begin{gathered}\frac{dq_i}{d\tau} = \mathrm{Re}\left(\frac{\partial H}{\partial p_i}\right)\left\{1 + \left[\frac{\mathrm{Im}(\partial H/\partial p_i)}{\mathrm{Re}(\partial H/\partial p_i)}\right]^2\right\}, \\ \frac{dp_i}{d\tau} = -\left[1 - j\frac{\mathrm{Im}(\partial H/\partial p_i)}{\mathrm{Re}(\partial H/\partial p_i)}\right]\frac{\partial H}{\partial q_i}.\end{gathered} \tag{11}$$

After changing to the complex geometrical optics, Eqs. (11) for the characteristics contain the additional terms.

$$\left[\mathrm{Im}(\partial H/\partial p_i)/\mathrm{Re}(\partial H/\partial p_i)\right]^2$$
$$\text{and } -j\,\mathrm{Im}(\partial H/\partial p_i)/\mathrm{Re}(\partial H/\partial p_i).$$

According to [13], a pulse is expressed via eikonal ψ as $p_i = \partial\psi/\partial q_i$. Therefore, taking (11) into account, we define a change in eikonal along each characteristic (a ray path) by the expression

$$\begin{gathered}d\psi/d\tau = \sum_{i=1}^{3}\frac{\partial\psi}{\partial q_i}\frac{dq_i}{d\tau} = \sum_{i=1}^{3} p_i\,\mathrm{Re}(\partial H/\partial p_i) \\ \times\left\{1 + \left[\mathrm{Im}(\partial H/\partial p_i)/\mathrm{Re}(\partial H/\partial p_i)\right]^2\right\}.\end{gathered} \tag{12}$$

Equations (11) and (12) form a complete characteristic system for used Eqs. (3) and (4) and pulse, which is used for either normal mode (both ordinary and extraordinary). The obtained system makes it possible to describe the formation of ray paths and absorption in a self-consistent manner (with regard to their mutual influence) as well as an inhomogeneous wave structure. We numerically integrated Eqs. (11) and (12), using the Runge–Kutta method in spherical geomagnetic coordinates. Along each ray path, the difference interval was selected variable and substantially smaller than the characteristic dimension of an inhomogeneity in the refractive index spatial distribution.

When solving this system, we should not solve the problem of an analytical continuation of the medium refractive index function into the region where the observation point radius vector values are complex. This is especially important when the wave propagation in 3D inhomogeneous mediums is numerically simulated. We consider only ray paths, which remain in an illuminated region, not going into the caustic shadow region. In the scope of a geometrical optics approximation, the solution to characteristic system (11) and (12) makes it possible to study self-consistently the mutual influence of the ray path, absorption, and wave inhomogeneous structure formation in mediums with not only weak but also strong absorption. Studying the HF radio wave propagation in the ionosphere can be one of the solution applications.

We study the influence of absorption on the ray path formation and the propagating wave structure inhomogeneity presented in [15]. The effects of medium anisotropy and wave dispersion are ignored here for clarity. The numerical calculations, performed based on the RWP model, indicated that (according to the known concepts) the plasma refractive index real part decreases and the imaginary part increases at each frequency in going deep into the ionospheric layer. This makes it possible to apply the following model of a medium. We introduce Cartesian coordinates x and z. A wave propagation medium is specified by the model of a limited parabolic layer with a complex refractive index:

$$\begin{gathered}n = n_1 + jn_2, \\ n_1^2(z) = b - (b - \varepsilon_{m1})\left[1 - \left(1 - \frac{z}{z_m}\right)^2\right], \quad 0 \le z \le 2z_m; \\ n_1^2(z) = b, \quad z < 0, \quad z > 2z_m, \\ n_2^2(z) = a + (\varepsilon_{m2} - a)\left[1 - \left(1 - \frac{z}{z_m}\right)^2\right], \quad 0 \le z < 2z_m; \\ n_2^2(z) = a, \quad z < 0, \quad z \ge 2z_m,\end{gathered} \tag{13}$$

where a, b, z_m, ε_{m1}, and ε_{m2} are the layer parameters.

We introduce the complex pulse vector (**p**) with Cartesian projections $p_x = p_{x1} + jp_{x2}$, $p_z = p_{z1} + jp_{z2}$ and the complex eikonal function $\psi = \psi_1 + j\psi_2$. If (13) is taken into account, the characteristic system has the following form in a complex geometrical optics

approximation with real ray paths in Cartesian coordinates (x, z):

$$dx/d\tau = p_{x1}\left[1+\left(p_{x2}/p_{x1}\right)^2\right],$$

$$dz/d\tau = p_{z1}\left[1+\left(p_{z2}/p_{z1}\right)^2\right];$$

$$\frac{dp_{x1}}{d\tau} = \frac{1}{2}\frac{\partial\left(n_1^2-n_2^2\right)}{\partial x}+\frac{p_{x2}}{p_{x1}}\frac{\partial\left(n_1n_2\right)}{\partial x},$$

$$\frac{dp_{z1}}{d\tau} = \frac{1}{2}\frac{\partial\left(n_1^2-n_2^2\right)}{\partial z}+\frac{p_{z2}}{p_{z1}}\frac{\partial\left(n_1n_2\right)}{\partial z};$$

$$\frac{dp_{x2}}{d\tau} = \frac{\partial\left(n_1n_2\right)}{\partial x}-\frac{1}{2}\frac{p_{x2}}{p_{x1}}\frac{\partial\left(n_1^2-n_2^2\right)}{\partial x},$$

$$\frac{dp_{z2}}{d\tau} = \frac{\partial\left(n_1n_2\right)}{\partial z}-\frac{1}{2}\frac{p_{z2}}{p_{z1}}\frac{\partial\left(n_1^2-n_2^2\right)}{\partial z};$$

$$\frac{d\psi_1}{d\tau} = p_{x1}^2+p_{x2}^2+p_{z1}^2+p_{z2}^2,$$

$$\frac{d\psi_2}{d\tau} = p_{x1}p_{x2}\left[1+\left(\frac{p_{x2}}{p_{x1}}\right)^2\right]+p_{z1}p_{z2}\left[1+\left(\frac{p_{z2}}{p_{z1}}\right)^2\right].$$

We integrate these equations, having applied layer model (13). We write x_0 and z_0 for point source coordinates, and $(p_{x1})_0$, $(p_{x2})_0$, $(p_{z1})_0$, and $(p_{z2})_0$ for the initial values of an extracted ray pulse. The integration of the equation characteristics gives $p_{x1} = (p_{x1})_0$, $p_{x2} = (p_{x2})_0$. Equation $p^2 = n^2$ follows from the eikonal equation and the characteristic system.

We now find

$$p_{z1}^2 - p_{z2}^2 = n_1^2 - n_2^2 - \left[\left(p_{x1}^2\right)_0 - \left(p_{x2}^2\right)_0\right],$$

$$p_{z1}p_{z2} = n_1n_2 - (p_{x1})_0(p_{x2})_0,$$

from which it follows that

$$p_{z1}^2 = \frac{1}{2}\left\{n_1^2-n_2^2-\left[\left(p_{x1}^2\right)_0-\left(p_{x2}^2\right)_0\right]\right\}+\left\{\frac{1}{4}\left\{n_1^2-n_2^2 - \left[\left(p_{x1}^2\right)_0-\left(p_{x2}^2\right)_0\right]\right\}^2+\left(n_1n_2-\left(p_{x1}\right)_0\left(p_{x2}\right)_0\right)^2\right\}^{1/2}.$$

Assume that $z_0 < 0$ and a distinguished ray is incident on a parabolic layer limited from below. Two cases are possible. In the first case, a ray is reflected from a layer at a point where

$$p_{z1}^2 = 0. \tag{14}$$

In such a case, we obtain the equations that can be satisfied at a ray reflection point (x_n, z_n):

$$\begin{aligned} n_1n_2 - \left(p_{x1}\right)_0\left(p_{x2}\right)_0 &= 0,\\ n_1^2 - n_2^2 - \left[\left(p_{x1}^2\right)_0 - \left(p_{x2}^2\right)_0\right] &\le 0. \end{aligned} \tag{15}$$

In the second case, the last conditions are not satisfied when a wave disturbance propagates along a ray, and a ray propagates through a layer without reflection. In this case the transformations give

$$dx/dz = \left\{(p_{x1})_0(p_{z1})^2\left[(p_{x1})_0^2+(p_{x2})_0^2\right]\right\} \times\left\{(p_{x1})_0^2p_{z1}\left[(p_{z1})^2+(p_{z2})^2\right]\right\}^{-1}.$$

In the first case, we obtain

$$x = x_0 + (p_{x1})_0\left\{1+\left[(p_{x2})_0/(p_{x1})_0\right]^2\right\} \times\left(\int_{z_0}^{z_n}\mp\int_{z}^{z_n}\right)dz\frac{p_{z1}^4}{p_{z1}\left\{p_{z1}^4+\left[n_1n_2-(p_{x1})_0(p_{x2})_0\right]^2\right\}},$$

where the subscript is taken if the finite integration point is located behind the reflection point in a distinguished ray; the lower symbol is taken if this point is before the turning point. It is evident that the path of each reflected ray is formed as a mirror reflection of the corresponding incident ray path relative to a straight line $(x = x_n)$. In the second case, the integration is performed from the initial value (z_0) to the finite value (z).

In a geometrical optics zero approximation, the harmonic wave electric field strength is written as

$$\begin{aligned}\mathbf{E}(\mathbf{r},t) &= \mathbf{E}_m(\mathbf{r})\exp\{j(k_0\psi(\mathbf{r})\}-\omega t)\\ &= \mathbf{E}_m(\mathbf{r})\exp\{-k_0\psi_2(\mathbf{r})\}\exp\{j(k_0\psi_1(\mathbf{r}))-\omega t\},\end{aligned}$$

where $\mathbf{E}_m(\mathbf{r})$ is the complex oscillation amplitude, ω is the oscillation frequency, k_0 is the wave number, $k_0 = \omega/c$, and c is the velocity of light. We define a length element along a distinguished ray:

$$ds = \left[(dx)^2+(dz)^2\right]^{1/2} = \left\{(p_{x1}^2)_0\left\{1+\left[(p_{x2})_0/(p_{x1})_0\right]^2\right\}^2 + p_{z1}^2\left[1+\left(p_{z2}/p_{z1}\right)^2\right]^2\right\}^{1/2}d\tau,$$

as well as the phase incursion and the integral absorption coefficient on the distinguished ray segment with length s:

$$k_0\psi_1(s) = k_0\int_0^s\frac{(p_{x1}^2)_0+(p_{x2}^2)_0+p_{z1}^2+p_{z2}^2}{\left\{(p_{x1}^2)_0\left\{1+\left[(p_{x2})_0/(p_{x1})_0\right]^2\right\}^2+p_{z1}^2\left[1+\left(p_{z2}/p_{z1}\right)^2\right]^2\right\}^{1/2}}ds,$$

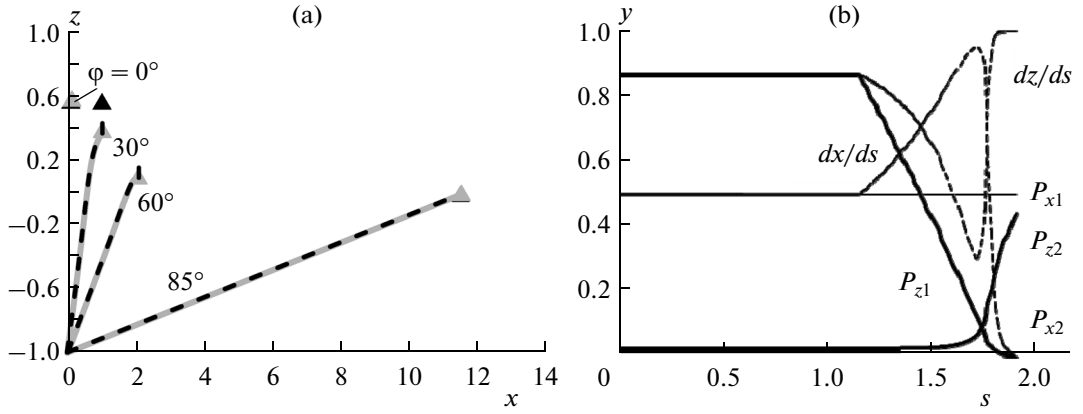

Fig. 2. Numerical calculation results: (a) ray paths without absorption (solid lines; $n_2 = 0$, $b = 1$, $\varepsilon_{m1} = -0.2$ and with regard to absorption (dashed lines; $a = 0.001$, $\varepsilon_{m2} = 0.0011$, $b = 1$, $\varepsilon_{m1} = 0.2$); reflection points of rays incident on a layer (triangles); black and gray colors indicate that absorption is present or absent, respectively. (b) Projections of the ray and pulse vectors for a ray (a dashed line for $\varphi_0 = 30°$ in Fig. 2a).

$$k_0\psi_2(s) = k_0\int_0^s \frac{(p_{x1})_0(p_{x2})_0\left\{1+\left[(p_{x2})_0/(p_{x1})_0\right]^2\right\} + p_{z1}p_{z2}\left[1+\left(p_{z2}/p_{z1}\right)^2\right]}{\left\{(p_{x1}^2)_0\left\{1+\left[(p_{x2})_0/(p_{x1})_0\right]^2\right\}^2 + p_{z1}^2\left[1+\left(p_{z2}/p_{z1}\right)^2\right]^2\right\}^{1/2}}ds.$$

We find the projections of the unit vector, which is tangential to the distinguished ray and shows the wave energy propagation direction:

$$\frac{dx}{ds} = \frac{(p_{x1})_0\left\{1+\left[(p_{x2})_0/(p_{x1})_0\right]^2\right\}}{\left\{(p_{x1}^2)_0\left\{1+\left[(p_{x2})_0/(p_{x1})_0\right]^2\right\}^2 + p_{z1}^2\left[1+\left(p_{z2}/p_{z1}\right)^2\right]^2\right\}^{1/2}},$$
$$\frac{dz}{ds} = \frac{p_{z1}\left[1+\left(p_{z2}/p_{z1}\right)^2\right]}{\left\{(p_{x1}^2)_0\left\{1+\left[(p_{x2})_0/(p_{x1})_0\right]^2\right\}^2 + p_{z1}^2\left[1+\left(p_{z2}/p_{z1}\right)^2\right]^2\right\}^{1/2}}. \quad (16)$$

We represent the complex pulse in the form $\mathbf{p} = p\mathbf{l}$, where p is the pulse complex value. The vector of normal $\mathbf{l}$ is complex and real for inhomogeneous and homogeneous waves, respectively. A homogeneous wave is a particular case of an inhomogeneous wave, when $(p_{x2}/p_{x1} = p_{z2}/p_{z1})$. The phase front of a homogeneous wave (in contrast to that of an inhomogeneous wave) propagates in the same direction as a ray front.

We consider the results of the numerical calculations (Fig. 2). Assume that a point source emits homogeneous harmonic waves. Source coordinates are: $x_0 = 0$, and $z_0 = -1$. The pulse projection initial values are: $(p_x)_0 = n(x_0, z_0)\cos\varphi_0$, $(p_z)_0 = n(x_0, z_0)\sin\varphi_0$, where φ_0 is the initial angle of incidence of the distinguished ray on a layer.

Figure 2a indicates that a ray penetrates deeper into a layer, if absorption is taken into account when a ray is obliquely incident on a plasma sheet. This effect weakens with increasing ray angle of incidence on a plasma sheet. A difference in the ray behavior between two studied cases increases with increasing depth of penetration into a plasma sheet. The numerical experiments indicate that such differences are substantial for the ionospheric $F2$ layer for the ionospheric propagation of short waves, especially under daytime conditions near a ray turning point, where the electron density and gradients are maximal. Figure 2b shows the variations in the ray vector (dx/ds, dz/ds) projections ($d\mathbf{r}/ds$) and in the pulse vector ($\mathbf{p} = \mathbf{p}_1 + j\mathbf{p}_2$) real ($p_{x1}, p_{z1}$) and imaginary ($p_{x2}, p_{z2}$) parts for the case when a ray is incident on a plasma sheet at an angle of $\varphi_0 = 30°$. The angle between the ray vector ($d\mathbf{r}/ds$) and the pulse real part vector ($\mathbf{p}_1$) increases as a distinguished ray penetrates deeper into a plasma sheet. A difference in the propagation direction and velocity of the phase and energy correspondingly increases. This means that a wave inhomogeneous structure develops. At the ray upper point (when the turning point is reached), a total internal reflection is achieved, when the indicated angle becomes equal to 90°. As a ray penetrates

deeper into a plasma sheet, $|\mathbf{p}_2|$ also increases since absorption becomes higher.

An analysis of the calculations makes it possible to draw the following conclusions:

1. The penetration of obliquely incident rays into a limited layer increases when absorption increases and the refractive index real part remains constant. The ray reflection from a layer can even change into the ray propagation through a layer. A complex geometrical optics changes into a usual one, if the effect of absorption on the formation of ray paths is ignored in Eqs. (11), when $n_2 = 0$. The conclusions are confirmed by an analysis of system (15).

2. The case of a normal ray incidence on a limited layer is an exception. A ray reflects at the same value, i.e., at $z = z_n$, when absorption is present and absent, other conditions being equal (Fig. 2a).

3. A homogeneous wave remains homogeneous when it propagates in a nonabsorbing layer. The vertical projections of the pulse vector and the vector tangential to a ray vanish at a reflection point (Fig. 2b). The latter follows from an analysis of expressions (14) and (16). The phase and ray wave fronts turn during the propagation.

4. Wave inhomogeneity increases during the penetration into an absorbing limited layer (Fig. 2b). A total internal reflection of an incident wave is reached at a reflection point. The vector of an obliquely incident wave pulse is directed here along the x axis, and the tangential vector is directed along the z axis. The incident wave energy flux is compensated upward by a reflected wave (see formula (16)).

3. MODEL DEVELOPMENT FOR THE PROPAGATION OF LFM PULSES IN THE IONOSPHERE

The RWP model for the case of wideband HF signals in the ionosphere was developed in [16]. A dynamic representation of LFM signals in the form of a wave packet sequence was used. The numerical model of the decameter signal propagation with linear frequency modulation (LFM pulses) was constructed. The model can be used to study the propagation of signals with different frequency band and a center spectral frequency in a 3D inhomogeneous anisotropic ionosphere. Dispersion distortions of LFM signals during their propagation in a 3D inhomogeneous anisotropic ionosphere were studied in [17].

We consider the emission of an LFM pulse by a transmitting antenna. This pulse is described by the mathematical model of the following form:

$$u(t) = 0, \quad t < 0, \quad t > \tau_u,$$
$$u(t) = A\exp\left\{-j\int_0^t(\omega_0 + \mu t)\,dt\right\}, \quad 0 < t < \tau_u, \tag{17}$$

where A is the pulse amplitude, τ_u is the pulse duration with an onset at $t = 0$, and ω_0 and μ are the frequency modulation parameters.

The discretization interval (Δt) is selected so that each train $u_\ell(t)$ of quasiharmonic oscillations with average frequency $\omega_{\ell+1/2}$ and a rectangular envelope would be a narrowband process. In this case the following inequalities are valid

$$\frac{2\pi}{\omega_{\ell+1/2}} \ll \Delta t \ll \frac{\omega_{\ell+1/2}}{\mu}, \quad \ell = 0,1,\ldots,(N-1).$$

At the lower boundary of the HF range, $\omega_0 = 6\pi \times 10^6$ 1/s and $2\pi/\omega_{1/2} = [3\times10^6(1 + k\Delta t/2\tau_u)]^{-1}$. If $k = 3$, $\tau_u = 10^{-4}$ s, and $\Delta t = 4\times10^{-6}$ s, $\Delta t\left(2\pi/\omega_{1/2}\right)^{-1} = 12.7$, and $\Delta t\left(\omega_{1/2}/\mu\right)^{-1} = 0.11$. An extracted LFM signal generates the emission of $N = \tau_u/\Delta t = 25$ wave packets.

The model can be used to study dispersion distortions of LFM pulses in an inhomogeneous anisotropic ionosphere. This model admits the generalization for other types of complex signals, e.g., for phase-shift keyed signals.

Figure 3 presents the results of some calculations in the case when the IRI model was used [12]. These calculations were performed for the conditions of the summer solstice at high solar activity ($F_{10.7} = 150$). Geographic coordinates of the selected hypothetical midlatitude transmitting station on the Earth's surface are 50° latitude and 290° longitude. We specified $\alpha = 90°$ and $\beta = 90°$. The results were achieved for an ordinary wave mode at 16:39 UT. In all cases we considered the emission of an LFM pulse, specified according to formula (17), by a transmitting antenna.

Figure 3 (left) shows the effective ray paths of extracted wave packets plotted in coordinates the geometric length (h) along the ray path–height above the Earth's surface (along the main ordinate axis). The differential absorption (k, dB km^{-1}) is also plotted in Fig. 3 as applied to the amplitudes of the rectangular envelopes of the same wave packets. A distortion of an individual wave packet form and dispersion splitting of ray path harmonic components are neglected. The current values of the presented length is $s_{pr} = ct_{gr}$, where t_{gr} is the group delay time of each wave packet from the emission point to the current point on a ray path.

Under the selected conditions, the critical frequency of the ionospheric $F2$ layer is in the frequency band of the specified LFM pulse. The plots are presented for four wave packets from the LFM pulse composition: with boundary center frequencies from the entire LFM pulse spectrum, with the lowest center frequency of a wave packet penetrating the ionosphere, and with the highest center frequency of a wave packet that still reflects from the ionosphere. Owing to ionospheric plasma dispersion, wave packets with different

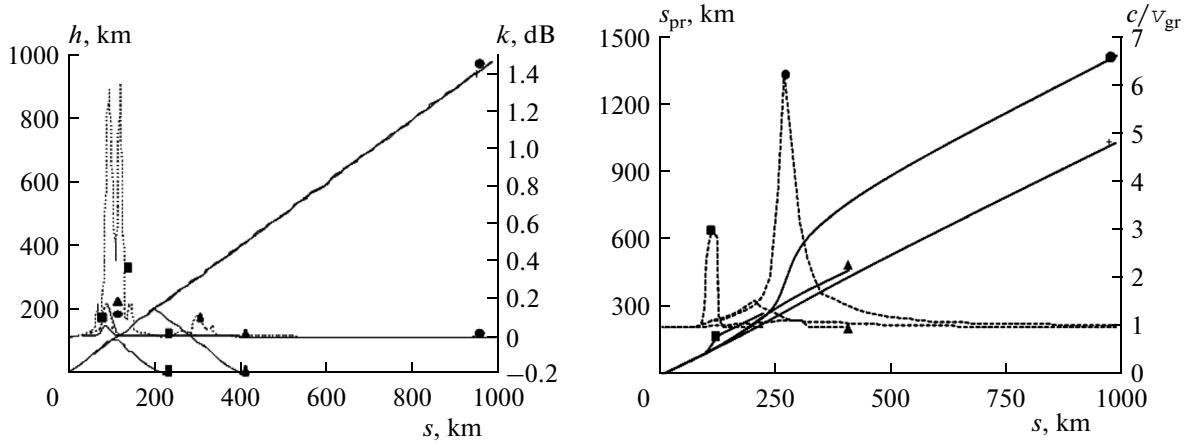

Fig. 3. Numerical calculations of the h, k, s_{pr}, and c/v_{gr} values depending on s for ordinary wave mode wave packets with 3.18 MHz (filled squares), 6.06 MHz (filled triangles), 6.42 MHz (filled circles), and 11.82 MHz (crosses) center frequencies in the LFM pulse composition during vertical sounding the ionosphere under daytime conditions.

carrier frequencies not only have different group velocities but also propagate along different ray paths. At an effective duration (Δt) of each wave packet, the packet length ($\Delta\sigma$) varies when it propagates in an inhomogeneous ionosphere along the corresponding ray path and for a weakly inhomogeneous medium $\Delta\sigma \approx v_{gr}\Delta t$.

The $c/v_{gr} \geq 1$ ratio for a distinguished wave packet increases, when a packet penetrates into the ionosphere, together with a decrease in the real part of the ionospheric plasma refractive index (n_1) and an increase in the wave packet absorption intensity. An increase in wave packet distortions is observed as its strong spreading along a path. Finally, the concept of a group velocity loses its meaning. In the calculations incorrect group velocity values $(c/v_{gr} < 1)$ can appear in the ionospheric regions where $n_1 < 0.3$. Such an effect is also more frequently observed for an ordinary wave mode than for an extraordinary one under the conditions when the geometrical optics is applicable. It becomes necessary to correct a model description of the wave packet propagation as compared to the description used above. The correction can be performed, e.g., based on a spectral approach.

The numerical calculations were also performed for other conditions in addition to those illustrated in Fig. 3 and in [17]. However, the main regularities in the manifestation of LFM pulse dispersion distortions in the ionosphere referred to above are general.

4. USAGE OF DIFFERENT MEDIUM MODELS AS THE NEXT STAGE IN THE RP MODEL DEVELOPMENT

The empirical models of the ionosphere (IRI) and neutral atmosphere (MSIS, Mass Spectrometer and Incoherent Scatter radar model [18]) were used in the RWP model version in order to describe a 3D inhomogeneous and anisotropic radiowave propagation medium. In this stage of the RWP model development, it became possible to use the data of the GSM TIP dynamic model of a medium in order to calculate the refractive index 3D distribution. The adaptation of the GSM TIP and IRI-2012 [19] calculation results to the RWP model for their joint usage consisted in the region separation from the global distribution of the medium parameters and in their 3D interpolation from the medium model grid nodes to each node along the radiowave propagation path. Such an adaptation made it possible to consider the HF radiowave propagation for two geomagnetic storms: on May 2–3, 2010 [20–22] and on September 26–29, 2011 [23, 24], with the medium parameters obtained in the results of the calculations performed using the GSM TIP and IRI-2012 models. Owing to the developed algorithm for deducing the electron density vertical profile for each node along a path, it became possible to represent the model calculation results in a fundamentally new form, which makes it possible to observe graphically the influence of a variable medium on the 3D propagation of HF radiowaves.

Figure 4 illustrates the numerical experiment of the ordinary mode propagation at 16:00 UT for quiet conditions on September 2011 during the main phase of the geomagnetic storm on September 26 and during the recovery phase on September 29. The coordinates of a hypothetic transmitting station were selected as follows: $\varphi = 11.2°$ S, $\lambda = 59.6°$ W (geographic coordinates); $\Phi = 0°$, $\Lambda = 10°$ (geomagnetic coordinates), so that radiowaves would propagate from the electron density trough region at the geomagnetic equator toward the equatorial anomaly northern crest (the azimuthal angle is $\beta = 0°$). We studied the influence of the variations in the medium parameters on different 13.5 MHz radiowave paths depending on the elevation angle that varies from 10° to 90° at an interval of 5°. We indicated two calculation versions for two models of a

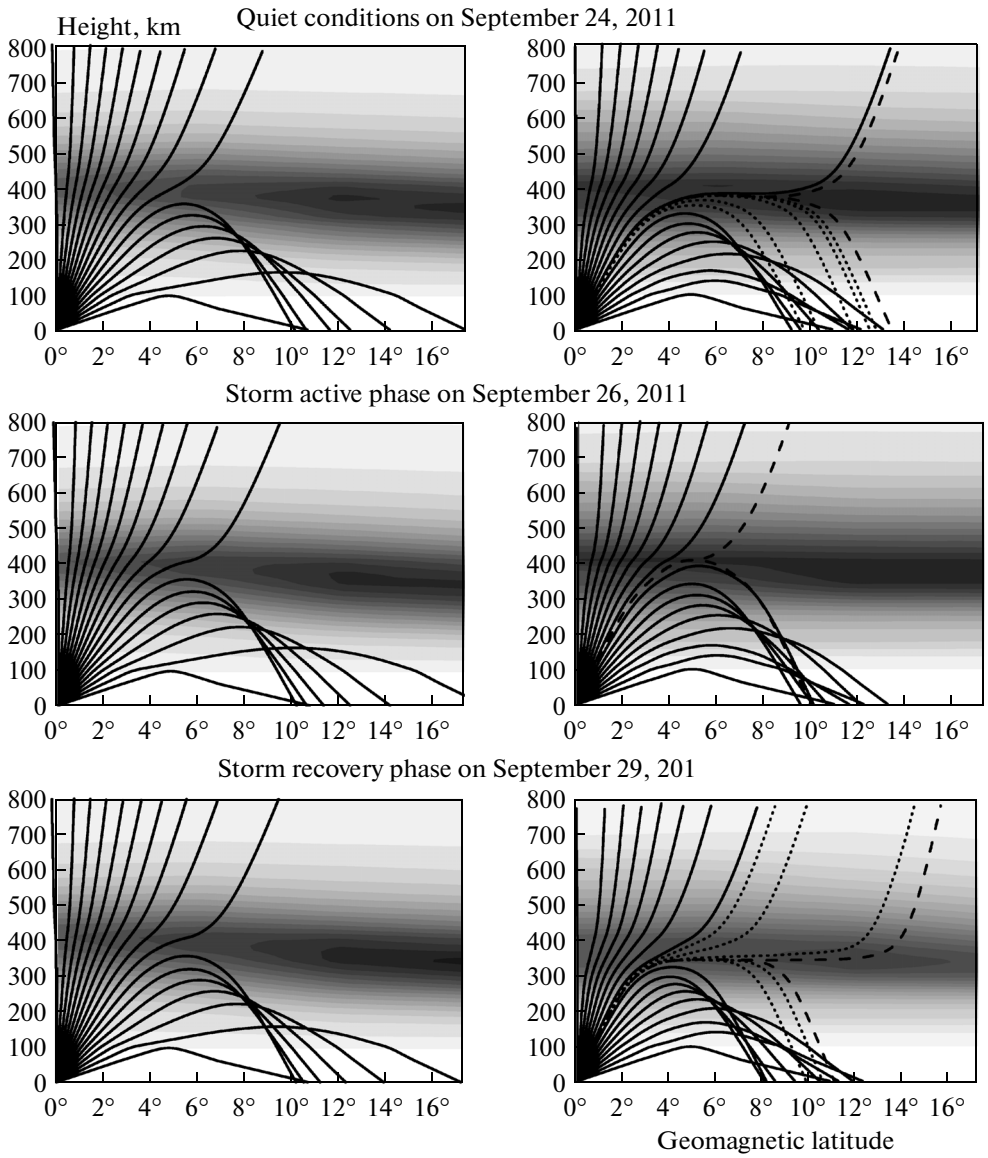

Fig. 4. Wave ray paths with $f = 13.5$ MHz, obtained in the IRI (left) and GSM TIP (right) models under quiet conditions during the main and recovery phases of the storm that occurred in 2011, against a background of electron density contour lines.

medium: IRI-2012 and GSM TIP. We indicated additional limiting cases of outgoing and reflected radiowaves, for which α differs by 0.005°, among the results of the calculations performed according to the GSM TIP model. We indicated additional lines for quiet conditions and the storm recovery phase in order to illustrate radiowave path variations depending on an elevation angle increment. It is evident that the Pedersen ray originated on those days in the calculation results.

CONCLUSIONS

Based on the aforesaid, we can make the following conclusions:

We presented the radiowave propagation model development for a complex geometrical optics and indicated that we can consider only rays that remain in an illuminated zone and do not fall in the geometrical shadow region, when real ray paths are used instead of complex paths. For the radio reception problems, when transmission and reception points are located in an illuminated region, paths entering into the shadow region are insignificant since a signal strongly attenuates when it falls in this region. The performed numerical calculations indicated that the numerical calculation results in the vicinity of the ray path turning point substantially change when we pass to a complex geometrical optics.

We developed the model for studying dispersion distortions of LFM pulses in a 3D inhomogeneous

anisotropic ionosphere. An approach to the dynamic representation of a complex signal by a wave packet sequence can be applied to not only LFM signals but also to other types of complex signals, e.g., to phase-shift keyed signals.

The adaptation of the operation of the RWP and GSM TIP models made it possible to study the variations in paths and their attenuations in the high-latitude, midlatitude, and low-latitude ionospheres under quiet geomagnetic conditions and during geomagnetic storms.

ACKNOWLEDGMENTS

This work was supported by the President of the Russian Federation, grant MK-4866.2014.5 (D.S. Kotova and M.V. Klimenko) and by the Russian Academy of Sciences, program 22 (V.V. Klimenko). The work was partially performed in the scope of the project "Physical Formation of the Response of the Upper Atmosphere and Ionosphere to the Processes in the Lower Atmosphere and on the Earth's Surface" (State Order of the Ministry of Education and Science of the Russian Federation, competitive part, order 3.1127.2014/K).

REFERENCES

1. M. Yu. Andreev, T. N. Lukicheva, and V. S. Mingalev, Geomagn. Aeron. **46**, 94 (2006).
2. M. Yu. Andreev, G. I. Mingaleva, and V. S. Mingalev, Geomagn. Aeron. **47**, 487 (2007).
3. M. Yu. Andreev, D. V. Blagoveshchenskii, V. M. Vystavnoi, V. S. Mingalev, and G. I. Mingaleva, Geomagn. Aeron. **47**, 502 (2007).
4. D. V. Blagoveshchensky, M. Yu. Andreyev, V. S. Mingalev, G. I. Mingaleva, and A. S. Kalishin, Adv. Space Res. **43**, 1974 (2009). doi:10.1016/j.asr.2009.01.030
5. G. V. Kotovich, V. P. Grozov, A. G. Kim, A. V. Oinats, E. B. Romanova, and A. V. Tashchilin, Geomagn. Aeron. **50**, 504 (2010).
6. A. A. Namgaladze, Yu. N. Koren'kov, V. V. Klimenko, et al., Geomagn. Aeron. **30**, 612 (1990).
7. M. V. Klimenko, V. V. Klimenko, and V. V. Bryukhanov, Geomagn. Aeron. **46**, 457 (2006).
8. V. E. Zakharov and A. A. Chernyak, Vestn. Ros. Gos. Univ. im. I. Kanta, No. 3, 36 (2007).
9. Yu. A. Kravtsov and Yu. I. Orlov, *Geometrical Optics of Inhomogeneous Media* (Nauka, Moscow, 1980), p. 304 [in Russian].
10. B. E. Brunelli and A. A. Namgaladze, *Physics of the Ionosphere* (Nauka, Moscow, 1988), p. 528 [in Russian].
11. D. S. Kotova, in *Step to Science*, Collection of Scientific Articles, No. 2: *Natural and Technical Sciences* (Kaliningrad, 2012), p. 42 [in Russian].
12. D. Bilitza, Radio Sci. **36**, 261 (2001).
13. Yu. A. Kravtsov and Yu. Ya. Yashin, Izv. Vyssh. Uchebn. Zaved., Radiofiz. **12**, 674 (1969).
14. V. E. Zakharov and E. N. Godovanaya, Vestn. Balt. Fed. Univ. im. I. Kanta, No. 4, 54 (2010).
15. V. E. Zakharov and E. N. Godovanaya, Vestn. Balt. Fed. Univ. im. I. Kanta, No. 4, 96 (2010).
16. V. E. Zakharov and D. S. Kotova, Radiotekhnika, No. 2, 87 (2013).
17. V. E. Zakharov and D. S. Kotova, Vestn. Balt. Fed. Univ. im. I. Kanta, No. 4, 34 (2013).
18. A. E. Hedin, J. Geophys. Res. A **96**, 1159 (1991).
19. D. Bilitza, D. Altadill, Y. Zhang, et al., J. Space Weather Space Clim. **4**, A07 (2014). doi:10.1051/swsc/2014004
20. D. S. Kotova, M. V. Klimenko, V. V. Klimenko, et al., in *Proceedings of the 18th Regional Conference on Propagation of Radio Waves* (St.-Petersburg, 2012), p. 72.
21. D. S. Kotova, M. V. Klimenko, V. V. Klimenko, and V. E. Zakharov, Vestn. Balt. Fed. Univ. im. I. Kanta, No. 4, 55 (2014).
22. D. S. Kotova, M. V. Klimenko, V. V. Klimenko, and V. E. Zakharov, Radiophys. Quantum Electron. **57**, 467 (2014).
23. D. S. Kotova, M. V. Klimenko, V. V. Klimenko, and V. E. Zakharov, in *Proceedings of the Baikal School on Fundamental Physics 2013 Physical Processes in Space and Near-Earth Media and 13th Conference of Young Scientists on Interaction of Fields and Radiation with Matter* (Irkutsk, 2013), p. 242.
24. D. S. Kotova, M. V. Klimenko, V. V. Klimenko, and V. E. Zakharov, in *Proceedings of the 19th Regional Conference on Propagation of Radio Waves* (St.-Petersburg, 2013), p. 54.

Translated by Yu. Safronov